Development of a Robust Class of Quasi-Poloidal Compact Stellarator Configurations

D. J. Strickler[1], S. P. Hirshman, D. A. Spong, M. J. Cole,
J. F. Lyon, B. E. Nelson, A. S. Ware, D. E. Williamson
Oak Ridge National Laboratory

April 7, 2003

[1]E-mail: stricklerdj@ornl.gov

Abstract

A compact quasi-poloidally symmetric stellarator plasma and coil configuration is described that has desirable physics and engineering properties and a very low aspect ratio plasma bounded by good magnetic flux surfaces both in vacuum and at $\langle\beta\rangle = 2\%$. The configuration is robust insofar as variations of the plasma β and consequent bootstrap current leave the bounding flux surface approximately unchanged, thus reducing active positional control requirements. This configuration was developed using a new computational method targeting good vacuum flux surfaces, as a measure of robustness, in the design of magnetic coils. The stellarator plasma and coil design code STELLOPT is used to vary the coil geometry, which produces plasma geometry and profiles that optimize plasma performance with respect to neoclassical transport, infinite-n ballooning stability up to $\langle\beta\rangle = 2\%$, and coil engineering parameters. The normal component of the vacuum magnetic field is simultaneously minimized at the full-beta plasma boundary.

I INTRODUCTION

Compact stellarators are toroidal confinement devices with low aspect ratio $A = \langle R \rangle / \langle a \rangle \leq 5$, a small number of toroidal field periods ($2 \leq N_p \leq 5$), and bootstrap current producing a small fraction of the magnetic rotational transform. Here $\langle R \rangle$ and $\langle a \rangle$ are the average major and minor radii of the noncircular and nonaxisymmetric stellarator plasma. Compact stellarators have been developed to combine the advantages of stellarators (in particular, steady-state operation and the avoidance of disruptions) and tokamaks (e.g., good particle and energy confinement at high beta) in a low aspect ratio plasma configuration. Specific examples are the National Compact Stellarator Experiment (NCSX) [1], a three field-period proof-of-principle device with $A = 4.4$, and the Quasi-Poloidal Stellarator (QPS) [2], a two field-period concept exploration experiment with $A = 2.7$.

Numerical optimizations of three-dimensional (3D) plasmas [3], and the magnetic coil systems required to support them [4, 5], have led to important advances in the design of high aspect ratio stellarators such as Wendelstein 7-X [6]. Recently, the stellarator optimization code STELLOPT [7] has been used for low aspect ratio NCSX and QPS designs to determine the shape of the outer magnetic flux surface, together with internal plasma pressure and current profiles, that produce desirable physics properties such as confined particle drift trajectories and plasma stability at $\langle \beta \rangle \sim 2 - 4\%$. The integration of the COILOPT coil model [8], which includes explicit representations for modular coils as well as coil geometry constraints, into the stellarator optimization package STELLOPT provides a unique and important computational tool for the design of compact stellarators. This self-consistent analysis ensures that physics and engineering criteria are simultaneously targeted in the full-pressure, full-current plasma/coil configuration. The analysis to date has been based on a local minimization method, a parallel version of the Levenberg-Marquardt algorithm [9], and is implemented only after separate plasma and coil optimizations have identified an initial configuration with promising physics and engineering properties. This merged optimization technique has led to successful designs for the quasi-axisymmetric NCSX and the quasi-poloidally symmetric QPS.

The merged STELLOPT/COILOPT design approach [10] simultaneously optimizes plasma properties together with coil engineering characteristics. For each evaluation of the physics and engineering targets, the equilibrium magnetic field is provided by the VMEC [11] code, which assumes the existence of nested, island-free magnetic flux surfaces. Following this analysis, two important stellarator design issues remain: 1) the existence of nested, nearly-integrable (non-ergodic), magnetic flux surfaces, and 2) the flexibility and robustness of the coil design with respect to variations of plasma profiles and coil currents. Original work [12] to reduce islands in vacuum, and more recent work [13] at nonzero beta, offer a solution to the first of these problems. Island reduction is routinely applied to candidate NCSX coil configurations. In this paper we propose a method that addresses the second issue. It is based on including – in addition to the usual plasma confinement and stability properties at the full value of

beta – a vacuum field condition that drives the combined optimization of the plasma and coil configuration into a region of parameter space with improved robustness and flexibility. In Sec. II the optimization of plasma and coils is reviewed and in Sec. III the vacuum field target is described. Application of the technique to designing a QPS with improved physics and engineering properties is presented in Sec. IV.

II INTEGRATED OPTIMIZATION OF PLASMA AND COILS

The compact stellarators and coils developed here were determined by a series of separate optimization steps. First a fixed-boundary plasma configuration was determined – independent of coils – using STELLOPT. This was followed by a COILOPT optimization to determine a candidate set of coils to approximately reproduce the desired plasma. These coils were subsequently refined by a combined plasma and coil optimization, using the merged STELLOPT/COILOPT code. The coils and plasma for the resulting compact stellarator are shown in Fig. 1. The QPS coil set consists of modular coils to provide the helical field, together with toroidal field (TF) coils and vertical field (VF) coils for configurational flexibility. The coil design is subject to engineering constraints such as minimum coil-coil and coil-plasma separation and minimum coil radius of curvature.

In the STELLOPT code, the optimization is formulated as a least-squares minimization of a target $\chi^2 = \Sigma\chi_i^2(\boldsymbol{x})$, where the individual components, χ_i, are generally nonlinear functions of the system state vector $\boldsymbol{x}$. Prior to merging with COILOPT, the state vector $\boldsymbol{x}$, whose components are the independent variables, included coefficients describing the magnetohydrodynamic (MHD) plasma equilibrium pressure and current profiles, as well as either 1) Fourier coefficients of the plasma shape, in the case of a fixed-boundary optimization, or 2) external coil currents, if the optimization was executed in free-boundary mode. The functions χ_i include both stellarator physics and coil engineering figures of merit that are evaluated numerically using a set of models dependent on the solution of a 3D plasma MHD equilibrium. For example, neoclassical transport in the low-collisionality $1/\nu$ regime is optimized using the NEO [14] code to evaluate a function χ_{NEO} targeting values of the effective ripple factor $\epsilon_{\text{eff}}^{3/2}$ on several magnetic flux surfaces. Subroutines interface each physics and engineering model with the optimization code, and several models (e.g., NEO, COBRA [15], NESCOIL [4], TERPSICHORE [16]) are executed through system calls from these subroutines. Data from these models is passed to the optimization code through files, therefore requiring minimal modification to the software provided by the model developer. This is computationally efficient because the time required for evaluation of the physics model is typically long compared to the file-based data transfer time. Parallelization [17] on high performance computers is simply implemented at the level of the optimization algorithm (e.g.,

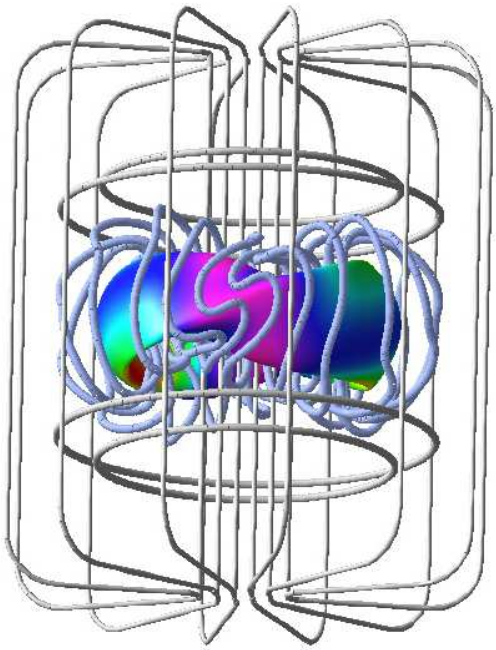

Figure 1: A compact QPS stellarator plasma and coil configuration. The colors indicate contours of constant $|\boldsymbol{B}|$ on the last closed flux surface. The plasma properties are predominantly determined by the nonplanar ("modular") coils surrounding the plasma. The circular coils above and below the plasma are the VF coils and the vertical coils are the TF coils.

computing the gradient of χ^2) and not within individual physics and engineering modules.

The COILOPT code [8] is based on a parametric representation of coils confined to a coil-winding surface (see Fig. 2) $R = \Sigma_i R_i \cos[2\pi(m_i u + n_i v)]$, $Z = \Sigma_i Z_i \sin[2\pi(m_i u + n_i v)]$, $\phi = 2\pi v/N_p$, where u and v are the normalized poloidal and toroidal angles, respectively. The winding law for modular coils on this surface (see Fig. 3) is described as a function of u and v by either Fourier series or a cubic spline representation $u(s) = \Sigma_j u_j B_j(s)$, $v(s) = \Sigma_j v_j B_j(s)$. In the spline representation, the basis functions $B_j(s) = B_j(s; t_j, \ldots, t_{j+4})$ are normalized cubic B-splines [18] defined on the interval $[0, 1]$ with a prescribed set of $N + 4$ non-decreasing knots $t_j \in [0, 1]$. The N pairs of coefficients (u_j, v_j) are referred to as "control points" (Fig. 3), and are constrained to satisfy periodic end conditions. Compared to the Fourier representation, splines allow control of *local* changes in coil geometry. Both the winding law coefficients and the coil currents are possible independent variables for coil optimization. The components of the objective function in COILOPT include penalty functions presenting the normal component of the magnetic field on the targeted plasma surface as well as engineering constraints on the coil geometry.

In the merged plasma/coil optimization code, the state vector $\boldsymbol{x}$ now consists of the independent variables from COILOPT (as described above), together with internal plasma profile coefficients from STELLOPT. In this merged model, COILOPT is executed in a "single-step" mode from a system call within STELLOPT to evaluate the coil-engineering contributions to χ^2. A solution is achieved by targeting *both* the physics parameters of the reference plasma *and* the geometric properties necessary for engineering coil design, while allowing the plasma boundary shape to vary in accordance with a free-boundary MHD equilibrium response to the external coils and currents.

III IMPLEMENTATION OF THE ROBUSTNESS (VACUUM FIELD) CONSTRAINT

Plasma flexibility and robustness are important components of stellarator coil design [19]. Of particular interest is the ability of a coil set to produce plasma configurations having a large fraction of nearly integrable surfaces over a wide range of β values. Since the plasma properties and surface quality are optimized at full β, there is no guarantee that the magnetic surface quality will be maintained at lower β. Indeed, the vacuum magnetic flux surfaces are typically evaluated by integration of the field line equations $dR/d\varphi = RB_R/B_\varphi$, $dZ/d\varphi = RB_Z/B_\varphi$ only *after* a coil configuration has been established by optimization at high beta.

Heretofore, it has been difficult to directly influence this important vacuum equilibrium feature during the optimization process. In this work, a vacuum field term $\chi_B = w_B|\boldsymbol{B} \cdot \boldsymbol{n}|/|\boldsymbol{B}|$ is added to the STELLOPT objective function χ^2 in an attempt to maintain flux surface integrity and robustness at low β.

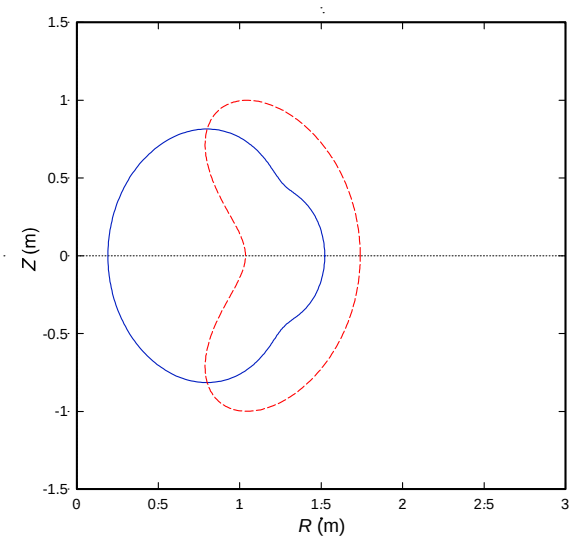

Figure 2: The coil winding surface shown in the v=0 (dashed) and v=1/2 (solid) toroidal symmetry planes.

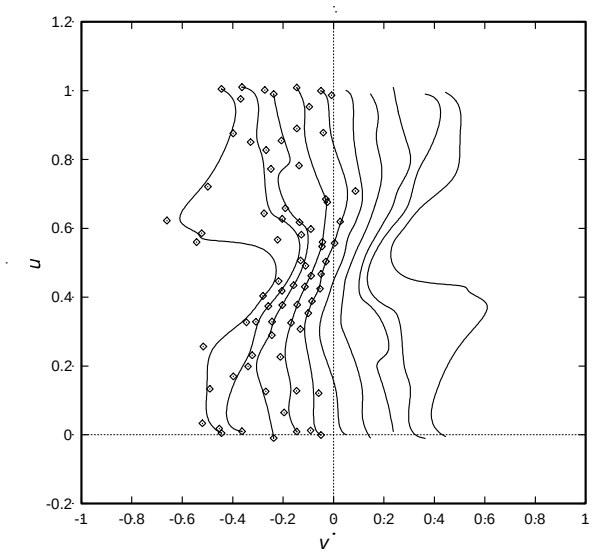

Figure 3: Filaments for 10 (of 20) QPS winding packs, depicting the modular coil winding law. The control points of the cubic B-splines are shown for the five unique winding pack types.

Here, $\boldsymbol{n}$ is the normal to the full-pressure plasma boundary, $\boldsymbol{B}$ is the *vacuum* magnetic field due to the coils, and w_B is the weight assigned to this target. During optimization, this term is minimized to force the last closed vacuum magnetic flux surface to enclose the same volume as the full-pressure plasma. Evaluation of this function requires knowledge of the plasma boundary. Thus, COILOPT is called twice for each evaluation of χ^2. The first call evaluates the coils needed to compute the free-boundary VMEC equilibrium. The next call then uses the computed plasma boundary to evaluate plasma-dependent constraints, including χ_B and the minimum plasma-coil distance.

Numerical experience shows that to obtain a plasma volume bounded by good vacuum flux surfaces that is comparable to that for the high β equilibrium requires an average error $\langle \delta B \rangle = (1/A) \int_{\partial P} |\boldsymbol{B} \cdot d\boldsymbol{A}|/|\boldsymbol{B}| \leq 1.3\%$ for the normal component of the vacuum magnetic field at the full-pressure plasma boundary ∂P.

IV DESIGN OPTIMIZATION FOR QPS

The QPS is a concept exploration experiment to investigate the effects of three-dimensional shaping and quasi-poloidal symmetry $\partial|\boldsymbol{B}|/\partial\theta \approx 0$ (θ is the poloidal angle in Boozer coordinates [20]) on neoclassical confinement at moderate β in a very low aspect ratio compact stellarator ($A \leq 2.7$). The QPS plasma has two field periods, average major radius $\langle R \rangle = 0.95$ m, volume averaged magnetic field $\langle B \rangle = 1$ T, and infinite-n ballooning stable limit $\langle \beta \rangle = 2\%$. The present nonplanar (modular) coil set in QPS consists of 20 modular coil winding packs (described below), 12 toroidal field (TF) coils capable of changing the toroidal field on axis by ± 0.2 T, and 2 pairs of circular vertical field (VF) coils. Additional engineering requirements for the QPS modular coils include a minimum space of 40 cm between the centerlines of coil winding packs across the center of the device for the TF legs and solenoid coils.

IV-A Coil Engineering Properties

The winding packs each contain multiple turns of multi-strand flexible copper conductor wound on a machined stainless steel winding form. In the present optimization, each winding pack was modeled with a single central filament. (Multi-filament, finite-build coils have been shown to have minimal effects on the physics properties of the QPS configurations.) Originally, the QPS modular coil set had 32 winding packs arranged in 16 coils of two winding packs closely separated by a thin structural "tee". Because of stellarator symmetry, there were only four different types of coils. An early innovation in the QPS design was to allow one of the four coil types (the coils nearest the center of the field period, or the $v = 1/2$ symmetry plane) to have winding packs that follow independent (non-parallel) paths (Fig. 4). This design featured a structural web that connected (mechanically, but not electrically) the two winding packs of the split coil and varied in width along the trajectory of the coil. This provided

the ability to create a more highly shaped magnetic field in the critical inboard region of the plasma near $v = 1/2$ without increasing either the total number of modular coils or the number of coil winding forms. Both of these are major cost drivers in compact stellarator coil design.

A recent change in the QPS coil design was to allow *all* pairs of winding packs to have this variable web structure, and to combine the winding packs *across* the $v = 1/2$ symmetry plane into a single stainless steel winding form. There are now two pairs of coils (winding packs) near the $v = 0$ symmetry plane which are wound on two spatially separated forms of the same type. This allows space near the $v = 0$ plane for diagnostic access to the plasma and reduces the number of distinct winding form types from 4 to 3 (Fig. 5). The total number of coil winding forms is decreased from 16 to 10 and the number of individual winding packs from 32 to 20. There are now five different coil types. These changes significantly reduce the cost of the modular coils, compared to the earlier design presented at the December, 2002 QPS Program Advisory Committee (PAC) meeting [2].

This new configuration was achieved by adding individual coil-to-coil spacing constraints in COILOPT. Previously, only a minimum distance $\Delta_n^{(min)}$ to all other coils was targeted for each of the different coil types. The new optimization targets a matrix of minimum coil separation constraints comparing each unique coil (winding pack) type n with a different coil $m \neq n$, i.e., $\chi_{n,m} = \max\{0, w_{n,m}(\Delta_{n,m}^{(target)} - \Delta_{n,m}^{(min)})\}$. Here, $w_{n,m}$ is the weight for this target. Thus, coils that are wound on the same winding form can be assigned a smaller separation target distance than those that are not joined by a structural web. This allows more spacing between coils in adjacent winding forms and the ability to orient the individual winding packs for improved fabricability.

Table 1 compares the re-configured coil system obtained using the vacuum field constraint (designated case 022103a), with the earlier QPS design [2]. Filamentary coils were used in the comparison. While both configurations have comparable aspect ratios ($\sim 2.65 - 2.75$), other plasma properties have improved in the present design. Plasma volume and ballooning-stable beta both increased. Neoclassical confinement in the $1/\nu$ regime, characterized here by the effective ripple at $r/a \sim 0.7$ (corresponding to the normalized toroidal flux $s = 0.5$), also improved, as indicated by a decrease in the ripple transport by a factor of ~ 2.6. This is directly correlated in QPS with a reduction of neoclassical poloidal viscosity, so the present design should allow greater control of the poloidal rotation needed for reduction of anomalous transport.

The coil engineering features of the new configuration are significantly improved (Table 1) compared to the PAC design. The minimum separation between the confined plasma and the coil centerline (plasma-coil separation), which is a measure of the plasma scrapeoff needed for adequate divertor operation, has increased by more than 2 cm ($\sim$18%). The minimum coil-coil separation is also larger, which allows the size and shape of the winding packs to be optimized for maximum conductor area. Preliminary layouts show that increased conductor area reduces the current density by $\sim$20%, which will in turn provide greater

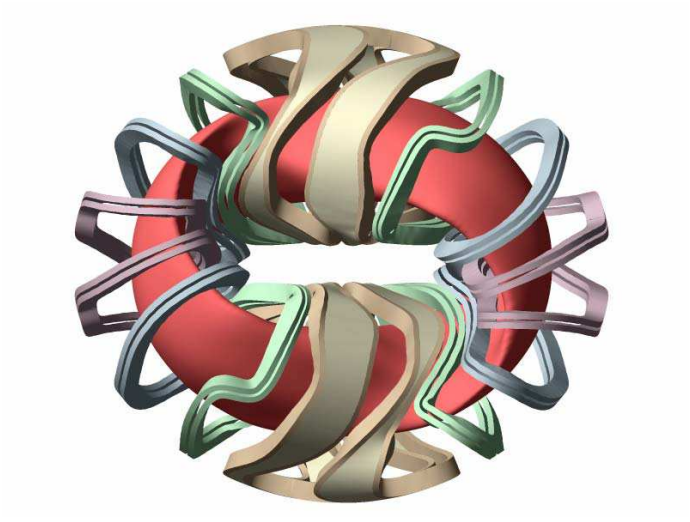

(a)

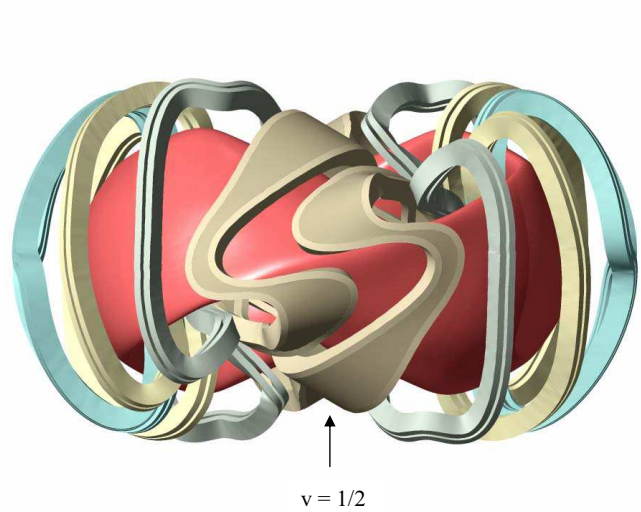

(b)

Figure 4: Top (a) and side view (b) of modular coils for the QPS PAC reference configuration [2]. Pairs of winding packs were joined by a structural web to form separate coils. All pairs of winding packs were closely spaced except those near the v=1/2 symmetry plane.

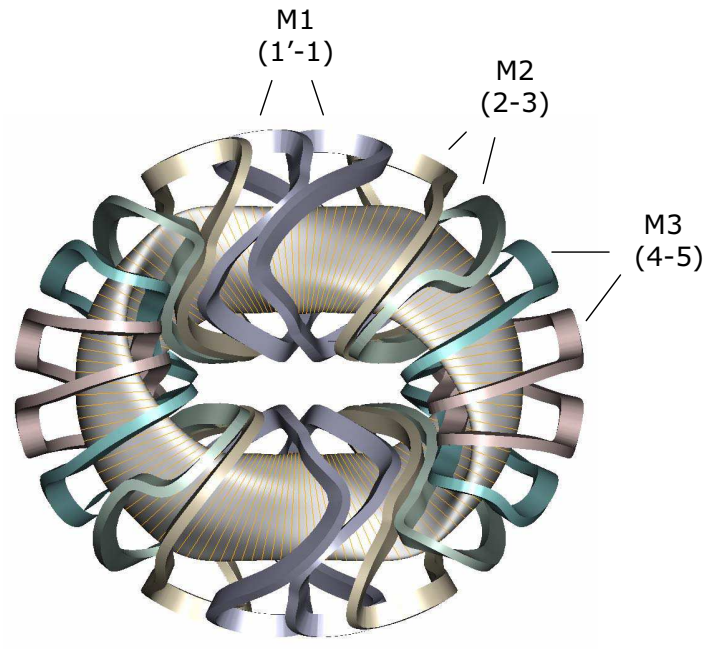

(a)

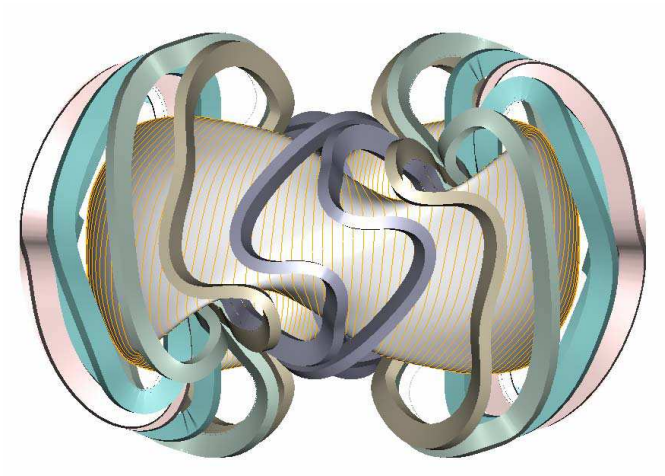

(b)

Figure 5: Top (a) and side view (b) of modular coils for the improved QPS configuration. Coil pairs 1' and 1, 2 and 3, and 4 and 5 are wound on the same winding form and are connected by a structural web (not shown) which varies in width along the coil trajectories.

experimental flexibility. The implied radial build indicates a scrapeoff distance of ~ 8 cm.

In addition to improved coil-coil separations, the new configuration also has a more uniform arrangement of "paired" and "unpaired" coils. This allows the twist of the coil cross section to more closely match a free-form or developable orientation [21]. The geometry of the supporting structure is also improved, with more space between coils in the region of the assembly joint of the two field periods. In the new configuration, the minimum distance across the center of the torus is larger by 4 cm. This space is used to accommodate the inner leg of the TF coils, the Ohmic solenoid, and vacuum casing. The additional space can be used to optimize the central structure and flux capability of the solenoid.

Other important parameters that have been considered in the optimization process are radius of curvature, or bend radius, of the winding center, total coil length, and overall dimensions of the coil set. In the new configuration, small increases in coil length and maximum major radius are offset by an increase in the minimum bend radius from 9.3 cm to > 12.2 cm. Bend tests with a prototypical conductor indicate that this change greatly improves the feasibility of winding coils without excessive distortion of the winding.

IV-B Magnetic Surface Quality

Vacuum magnetic surfaces for the new configuration are compared with those of previous designs in Figs. 6 - 8, which show the surfaces in the $v = 1/2$ symmetry plane. The PAC design was chosen for its low aspect ratio in both vacuum (Fig. 6) and at finite β, as well as good transport and stability characteristics. Optimization of this configuration to improve its coil-engineering properties *without* applying the vacuum constraint produced a plasma with a substantially smaller volume of nested magnetic surfaces (Fig. 7).

In the new configuration (Fig. 8), the vacuum normal field error has been significantly reduced at the location of the full beta boundary (see Table 1). (The coil currents are the same as those for the full beta case and were not further optimized for low beta.) This produced a plasma volume in vacuum that is comparable to, or larger than, that of the full-beta case and which exhibits a large fraction of closed magnetic surfaces (compared to islands). The average low-beta plasma radius can exceed 40 cm compared to 34 cm for the full-beta configuration. This preservation of aspect ratio with beta is important, since QPS experiments that focus on neoclassical transport reduction will be conducted at low beta. A small $n = 2, m = 9$ island chain is seen in Fig. 8. Island chains such as this may be targeted through the variation of coil currents (within the bounds set by power supply capability) and, if necessary, the addition of small correction coils. Magnetic islands do not seem to be an issue at higher beta. There is no low order resonant surface in the plasma at full beta. A recent PIES calculation [22] shows only a small $n = 6, m = 19$ island chain in the plasma and an outer flux surface that is larger than the original VMEC surface. In addition, the equilibrium bootstrap current is lower in the new configuration despite the higher beta and larger plasma volume, so there is a

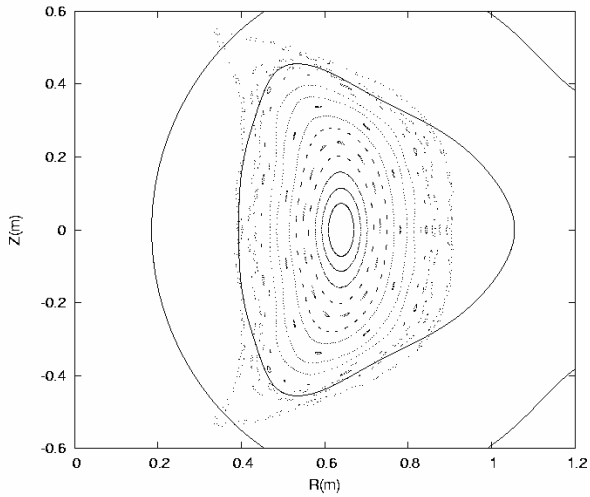

Figure 6: Vacuum magnetic surfaces in the v=1/2 symmetry plane for the QPS PAC configuration. The outer solid line is the coil winding surface and the inner solid line is the full-beta VMEC plasma boundary.

smaller difference between the iota profiles at low and full beta, as shown in Fig. 9.

IV-C Transport Properties

The achievement of low levels of neoclassical transport has been one of the important targets in our physics optimization. To verify that the new configuration described in Table 1 meets this goal, we have evaluated its transport properties using several different tools and compared the results with the earlier PAC reference design.

One of the significant ways in which stellarator transport differs from that in axisymmetric tokamaks is in the low collisionality regime where neoclassical transport coefficients in the stellarator scale as $1/\nu$ (until non-local super-banana effects become dominant at very low collisionality). In contrast, tokamak trans-

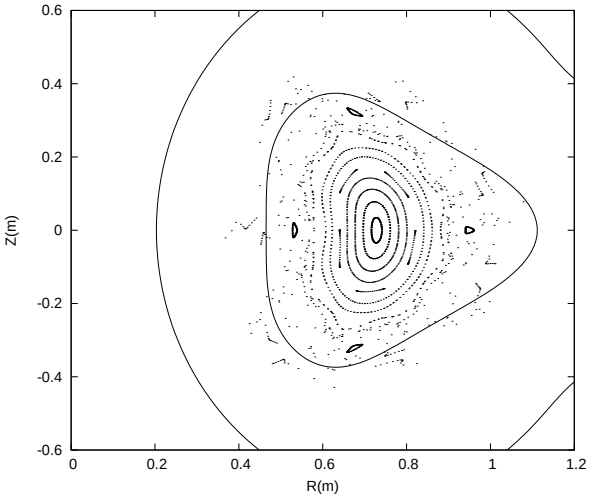

Figure 7: Vacuum magnetic surfaces in the v=1/2 symmetry plane for coils with improved physics properties *before* application of the vacuum constraint. The outer solid line is the coil winding surface and the inner solid line is the full-beta VMEC plasma boundary.

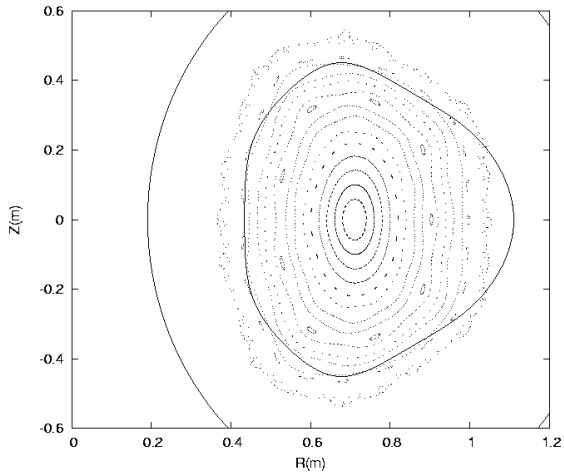

Figure 8: Vacuum magnetic surfaces in the v=1/2 symmetry plane for the improved coil (and physics) configuration (case 022103a), after applying the vacuum constraint. The outer solid line is the coil winding surface and the inner solid line is the full-beta VMEC plasma boundary.

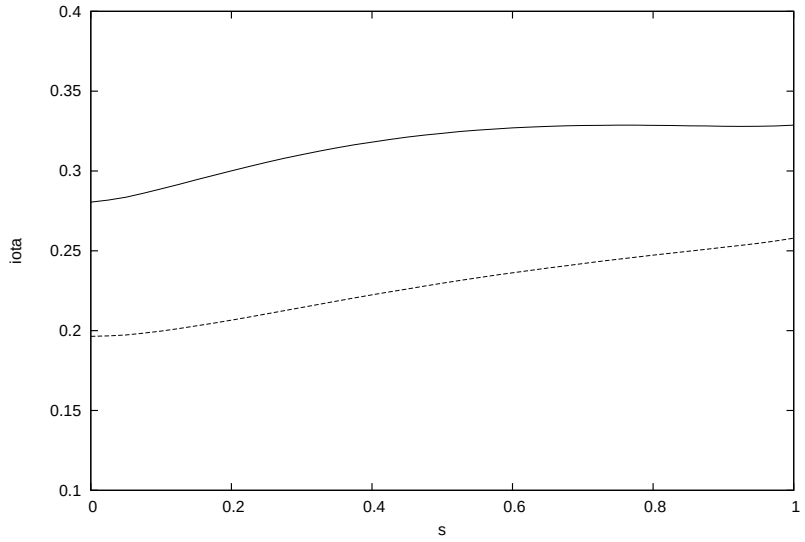

Figure 9: Iota profiles for the present QPS coil configuration *vs.* the normalized toroidal flux s for vacuum (dashed) and $< \beta >= 2\%$ (solid).

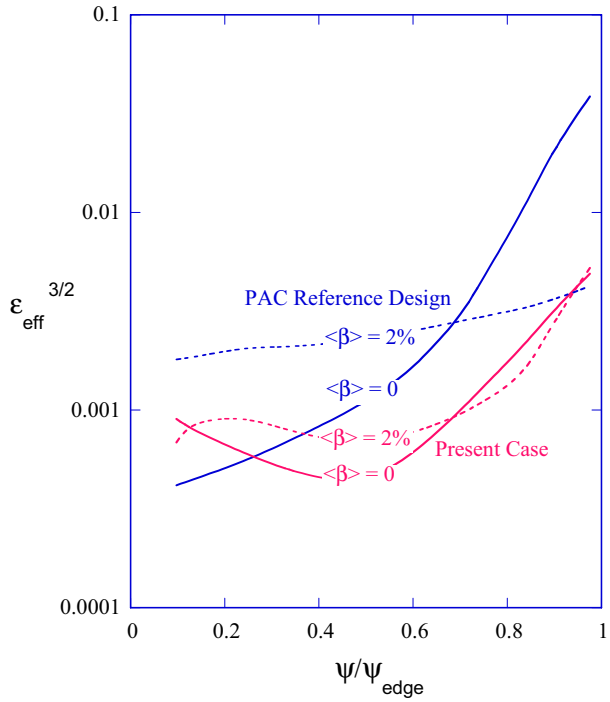

Figure 10: Effective ripple coefficient $\epsilon_{\rm eff}^{3/2}$ calculated from the NEO [14] code vs. normalized flux (radial position) for the present QPS configuration and the PAC reference case.

port coefficients continue to decrease as ν at low collisionalities. The overall level of the $1/\nu$ transport is determined by the effective ripple $\epsilon_{\rm eff}^{3/2}$. In designing low aspect ratio configurations, it has thus been desirable to minimize this effective ripple. The NEO [14] code has provided a rapid and accurate means for evaluating the level of ripple for an arbitrary spectrum of the magnetic field strength $|B|$. A plot of the effective ripple coefficients for the present QPS and the earlier PAC designs is shown in Fig. 10. There is a significantly lower ripple level over most of the plasma cross section in the present configuration.

An alternative way of evaluating transport in non-axisymmetric systems is to use Monte Carlo calculations that follow a large number of particle orbits in time and record the loss rates as the particles exit the plasma volume. The global particle and energy lifetimes can then be estimated by recording the energy lost as particles leave the confined volume and then reseeding them back into the plasma according to a probability distribution function that models

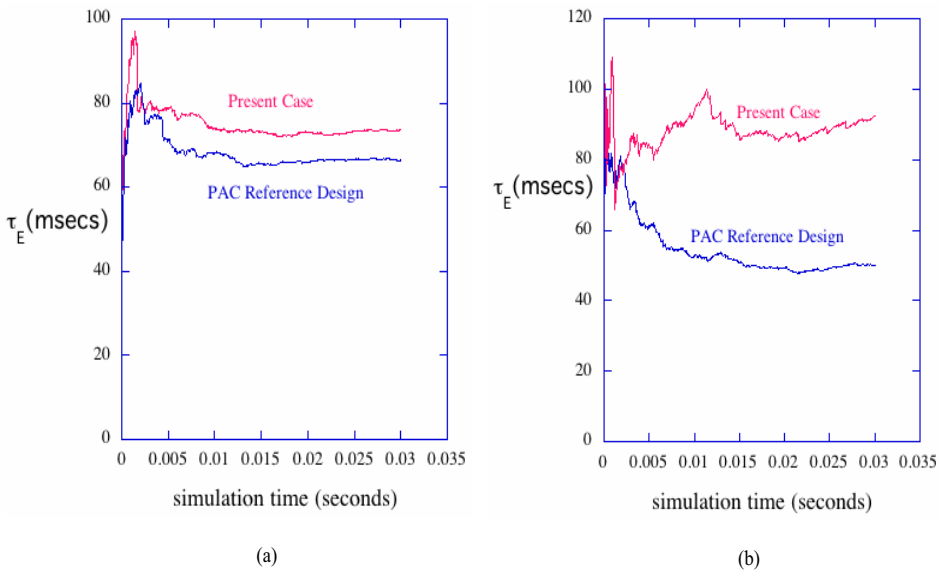

Figure 11: Monte Carlo thermal ion energy lifetimes for the present configuration and the PAC reference case based on (a) ICH regime parameters, and (b) ECH parameters.

prescribed temperature and density profiles. Such a calculation runs until the losses reach a quasi-steady state. In Figs. 11(a)-(b) such a model was applied to compute the thermal ion confinement in the two QPS devices described in Table 1. In Fig. 11(a), plasma parameters that characterize an ICRF-heated regime are used: $n(0) = 8.3\times10^{19}$ m^{-3}, $T_{ion}(0) = 500$ eV, $T_{electron}(0) = 500$ eV. In Fig. 11(b) plasma parameters that characterize a lower density ECRF-heated regime are used: $n(0) = 1.8 \times 10^{19}$ m^{-3}, $T_{ion}(0) = 150$ eV, $T_{electron}(0) = 1400$ eV. In both regimes, the present configuration offers higher energy confinement times than the earlier PAC device.

A unique physics feature of the QPS device arising from its quasi-poloidal symmetry is a much lower level of viscous flow damping in the poloidal direction as compared to the flow damping in the toroidal direction. This viscous anisotropy is reversed compared to that in a tokamak, which is characterized by a toroidal viscosity that is much lower than the poloidal viscosity. As a result of the connection between the poloidal viscosity and the generation of the sheared flows that are thought to be necessary for enhanced confinement regimes, QPS configurations may offer improved access to such regimes. Recently, a theoretical framework has been developed [23] that allows the calculation of the viscosity tensor coefficients for non-axisymmetric systems using the DKES [24]

neoclassical transport model. We have applied this formulation to the QPS configurations discussed above to compute the normalized viscosity coefficient profiles shown in Fig. 12. These coefficients relate the flux-surface averaged poloidal and toroidal components of the viscous stresses to the in-surface, averaged components of the flow velocity through the following equations:

$$\begin{pmatrix} \langle \boldsymbol{B}_P \cdot \nabla \cdot \boldsymbol{\pi} \rangle \\ \langle \boldsymbol{B}_T \cdot \nabla \cdot \boldsymbol{\pi} \rangle \end{pmatrix} = \begin{bmatrix} M_{PP} & M_{PT} \\ M_{TP} & M_{TT} \end{bmatrix} \begin{pmatrix} \langle u^P \rangle \\ \langle u^T \rangle \end{pmatrix} \tag{1}$$

For i (and j) $\in (P, T)$, M_{ij} are the coefficients M_{a1ij} given in Eq. (39) of Ref. [23] (with a = ion) in terms of the normalized viscosity coefficients $M'_{ij} \equiv M_{aij}(K)/4\pi^2 m_a v_{Ta} K^{3/2}$, where $K = E/T_a$ is the normalized particle energy. Here, $u^P = \boldsymbol{u} \cdot \nabla\theta/\chi'$ and $u^T = \boldsymbol{u} \cdot \nabla\zeta/\psi'$) are the normed poloidal and toroidal flows, respectively.

For both configurations, the poloidal viscosity coefficient (M'_{PP}) is substantially less than the toroidal viscosity coefficient (M'_{TT}). This is a direct consequence of attempting to impose quasi-poloidal symmetry on the spectrum of $|B|$ during the optimization. The present configuration has a higher ratio between the toroidal and poloidal viscosities than the PAC configuration (this ratio should approach ∞ for a perfectly quasi-poloidal symmetry design).

IV-D Stability Properties

The optimization included stability targets for both Mercier (interchange) and infinite-n ballooning at $\langle\beta\rangle \sim 2\%$. These were computed numerically using the COBRA code [15]. Stability to finite-n ballooning modes, as well as kink and vertical modes, was evaluated (as a post-processing calculation) using the TERPSICHORE code [16].

A fixed pressure profile, $p(s) = p_0 (1 - s)^2$, was used during the optimization process to test the stability of all configurations. Stability β limits for both QPS cases may be raised (to $\beta \sim 2.4\%$) by allowing small variations of the pressure profile. For the unoptimized pressure profile, the PAC reference case becomes unstable to infinite-n ballooning modes at $\langle\beta\rangle = 2.1\%$ and the present case at $\langle\beta\rangle = 1.9\%$. For finite-$n$ ballooning modes, the β limits are higher: $\langle\beta\rangle \sim 2.5\%$.

Kink and vertical modes become unstable for these types of QPS plasmas for even larger pressures: $\langle\beta\rangle \sim 4\%$.

SUMMARY

The capability for numerical optimization of high beta compact stellarator plasmas and coils has been extended through the implementation of a vacuum field constraint in the STELLOPT/COILOPT plasma and coil optimization code. In addition to the existing measures of plasma stability and transport at a reference value of beta, and engineering design constraints on coil geometry, this new target minimizes the normal component of the vacuum magnetic field at

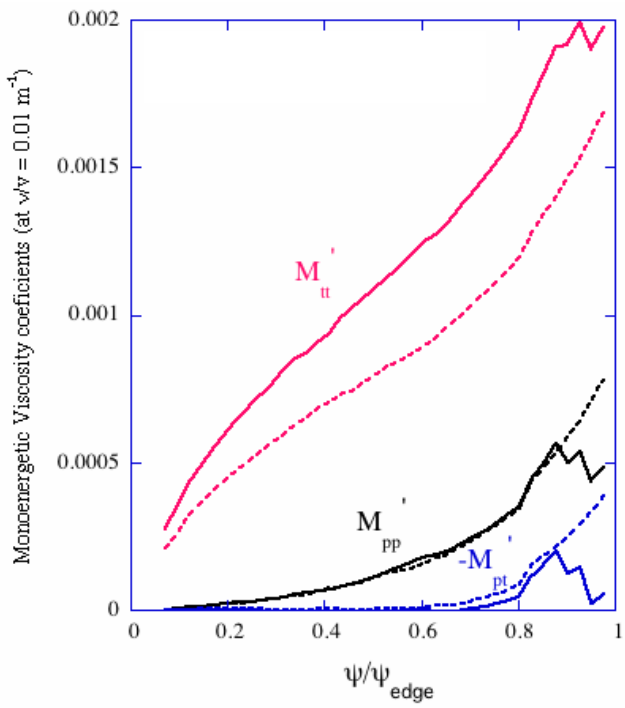

Figure 12: The components of the viscosity tensor $M'_{tt}, M'_{pt}, M'_{pp}$ for a fixed energy corresponding to $\nu/v = 0.01\ m^{-1}$ vs. flux surface position for the present QPS configuration (solid lines) and the PAC reference case (dashed).

the full-pressure plasma boundary. This minimization serves to guide the solution into a new region of parameter space where, in addition to good plasma and coil properties at the reference beta, the last closed vacuum magnetic flux surface encloses a large plasma volume. This vacuum field constraint, together with recent changes in the coil model, has resulted in an improved plasma and coil configuration for the Quasi-Poloidal Stellarator. The configuration shows some of the invariance to beta changes exhibited by the W7-X design [6], while preserving the ability to sustain nonzero bootstrap currents.

ACKNOWLEDGMENTS

The submitted manuscript has been authored by a contractor of the U.S. Government under contract No. DE-AC05-00OR22725. Accordingly, the U.S. Government retains a nonexclusive, royalty-free license to publish or reproduce the published form of this contribution, or allow others to do so, for U.S. Government purposes. We thank Dr. J. A. Rome for carefully reading the manuscript and providing helpful comments.

References

[1] G. H. Neilson, et al.,"Physics issues in the design of high-beta, low-aspect-ratio stellarator experiments", *Phys. Plasmas*, **7**, 1911 (2000).

[2] J. F. Lyon, et al., "Physics Issues for a Very-Low-Aspect-Ratio Quasi-Poloidal Stellarator (QPS)", 19th IAEA Fusion Energy Conference, Lyon, France (October, 2002), to be published.

[3] J. Nührenberg and R. Zille, *Phys. Lett. A*, **114**, 129 (1986).

[4] P. Merkel, *Nucl. Fusion*, **27**, 5, 867 (1987).

[5] M. Drevlak, *Fusion Technol.*, **33**, 106 (1998).

[6] G. Grieger, et al., *Proc. 13th Int. Conf. Plasma Physics and Nuclear Fusion Research*, Washington, D.C., October 1-6, 1990, Vol. 3, p. 525, International Atomic Energy Agency (1991).

[7] D. A. Spong, et al., *Nucl. Fusion*, **41**, 711 (2001).

[8] D. J. Strickler, L. A. Berry, and S. P. Hirshman, *Fusion Sci. and Technology*, **41**, 107 (2002).

[9] J. J. Moré, B. S. Garbow, and K. E. Hillstrom, "Users Guide to MINPAC-I," Argonne National Laboratory (1980).

[10] D. J. Strickler, L. A. Berry, S. P. Hirshman, et al., "Integrated Plasma and Coil Optimization for Compact Stellarators," 19th IAEA Fusion Energy Conference, Lyon, France (October, 2002).

[11] S. P. Hirshman and J. C. Whitson, *Phys. Fluids*, **26**, 3553 (1983).

[12] J. R. Cary and J. D. Hanson, *Phys. Fluids*, **29** 2464 (1986).

[13] S. R. Hudson, et al., *Phys. Rev. Lett.*, **89** 275003 (2002).

[14] V. V. Nemov, et al., *Phys. Plasmas*, **6**, 4622 (1999).

[15] R. Sanchez, et al., *J. Comput. Phys.*, **161**, 576 (2000).

[16] D. V. Anderson, et al., Int. *J. Supercomput. Appl.*, **4**, 34 (1990).

[17] D. A. Spong, et al., "QPS Plasma and Coil Optimization," 13th International Stellarator Workshop, Canberra, Australia (February, 2002).

[18] C. de Boor, "A Practical Guide to Splines," Springer-Verlag (1978).

[19] N. Pomphrey, et al., "Flexibility and Robustness Calculations for NCSX," Princeton Plasma Physics Laboratory Report PPPL-3701 (June, 2002).

[20] A. H. Boozer, "Plasma equilibrium with rational magnetic surfaces", *Phys. Fluids*, **24**, 1999 (1981).

[21] P. L. Walstrom, "Twisted Coil Geometry in Plasma Confinement Devices", *J. of Fusion Energy*, **3**, 265 (1987).

[22] D. Monticello, private communication (2003).

[23] H. Sugama, S. Nishimura, "How to calculate the neoclassical viscosity, diffusion, and current coefficients in general toroidal plasmas", *Phys. Plasmas*, **9**, 4637 (2002).

[24] W. I. van Rij, S. P. Hirshman, "Variational bounds for transport coefficients in three-dimensional toroidal plasmas", *Phys. Fluids B*, **1**, 563 (1989).

Target	**PAC Reference**	**Present Case**
A, aspect ratio	2.65	2.76
Volume (m^3)	1.81	2.27
Bootstrap current (kA)	45.9	37.8
Ballooning beta – infinite n (%)	1.83	2.00
Ripple diffusion $\times 10^3$ (s=0.5)	3.53	1.35
Iota at maximum β		
s=0	0.293	0.281
s=0.5	0.341	0.324
s=1.0	0.345	0.329
Normal Vacuum field error (%, s=1)		
Average	1.82	1.27
Maximum	6.45	4.34
Min. coil-plasma separation (cm)	13.0	15.4
Min. coil separation (cm)		
Winding pack 1′-1	14.9	9.4
Winding pack 1-2	6.1	13.0
Winding pack 2-3	9.6	10.4
Winding pack 3-4	11.0	13.1
Winding pack 4-5	13.8	13.9
Winding pack 5-5′	18.0	18.1
Min. radius of curvature (cm)		
Winding pack 1	9.3	12.8
Winding pack 2	9.4	12.3
Winding pack 3	11.0	12.2
Winding pack 4	12.4	15.3
Winding pack 5	14.2	16.4
Total coil length (m)	90.4	101.6
Max. coil R (m)	1.64	1.73
Min. distance across center, Y (cm)		
Winding pack 1	36.0	40.0
Winding pack 2	37.0	43.4
Winding pack 3	38.2	40.0

Table 1: Comparison of an improved QPS plasma and coil optimization (case 022103a) with the reference configuration presented at the December, 2002 PAC meeting. Distances are to the center of the winding packs, and ripple diffusion is in arbitrary units.